Electronic Supplementary Material (ESI) for Chemical Communications.

Bioinspired, ATP-Driven Co-operative Supramolecular Polymerization and its Pathway Dependence

Ananya Mishra, [a] Divya B. Korlepara,[b] Sundaram Balasubramanian [b] and Subi J. George *[a]

[a]Supramolecular Chemistry Laboratory, New Chemistry Unit, Jawaharlal Nehru Centre for Advanced Scientific Research (JNCASR), Jakkur, Bangalore, 560064, India.

Email: george@jncasr.ac.in

[b]Molecular Simulations Laboratory, Chemistry and Physics of Materials Unit, Jawaharlal Nehru Centre for Advanced Scientific Research, (JNCASR), Jakkur, Bangalore 560064, India.

Table of Contents

1. General Methods

NMR Measurements: NMR spectra were recorded with a Bruker AVANCE 400 (400 MHz) Fourier transform NMR spectrometer with chemical shifts reported in parts per million (ppm) with respect to TMS. Splitting patterns are designated as s, singlet; d, doublet; bs, broad singlet; m, multiplet; t, triplet; q, quartet; quin, quintet and br, broad.

High-Resolution Mass Spectrometry (HR-MS): High-Resolution Mass Spectra (HR-MS) were recorded on an Agilent 6538 Ultra High Definition (UHD) Accurate -Mass Q-TOF-LC/MS system using electrospray ionization (ESI) mode.

Matrix-Assisted Laser Desorption Ionization (MALDI): MALDI was performed on a Bruker daltonics Autoflex Speed MALDI TOF System (GT0263G201) spectrometer using α-Cyano-4-hydroxy-cinnamic acid (CCA) as the matrix.

Optical Measurements: Electronic absorption spectra were recorded on a Perkin Elmer Lambda 900 UV-Vis-NIR Spectrometer. Circular Dichroism (CD) spectra and temperature-dependent CD spectra were recorded on a Jasco J-815 spectrometer where the sensitivity, time constant and scan rate were chosen appropriately. The temperature dependent measurements were performed with a CDF-426S/15 Peltier-type temperature controller with a temperature range of 263-383 K and adjustable temperature slope. Emission spectra were recorded on Perkin Elmer LS 55 Luminescence Spectrometer. 10 mm x 10 mm quartz cuvettes were used for measurements.

Transmission Electron Microscopy (TEM): TEM measurements were performed on a JEOL, JEM 3010 operated at 300 kV. Samples were prepared by placing a drop of the solution on carbon-coated copper grids followed by drying at room temperature. The images were recorded with an operating voltage of 300 kV.

Scanning Tunnelling Electron Microscopy (STEM): STEM measurements were performed on a NOVA NANO SEM 600 (FEI) by putting a drop of the solution on carbon-coated copper grids and dried at room temperature and was operated with an accelerating voltage of 30 kV.

Dynamic light scattering Experiments (DLS): The measurements were carried out using a NanoZS (Malvern UK) employing a 532 nm laser at a back scattering angle of 173^{o}. The samples were measured in a 10 mm glass cuvette.

Confocal microscopy: Confocal microscopy imaging was done at room temperature using a Zeiss LSM 510 META laser scanning confocal microscope. The microscope objective of 63X (NA 1.4) and 100X (NA 0.5) were employed. Samples were prepared by dropping the solution on a glass slide and measurements were done in liquid state by following the standard procedure.

AFM: AFM measurements were performed on a Veeco diInnova SPM operating in tapping mode regime. Micro - fabricated silicon cantilever tips doped with phosphorus and with a frequency between 235 and 278 kHz and a spring constant of 20-40 Nm^{-1} were used. The samples were prepared by drop casting the solution of ATP bound **Amph-NDG** on silicon substrate and dried in air followed by vacuum drying at room temperature.

2. Synthetic Schemes and Procedures

The synthesis of **Amph-NDG** is shown in scheme S1.

Materials: All chemicals were purchased from commercial suppliers and were used directly without any further purification.

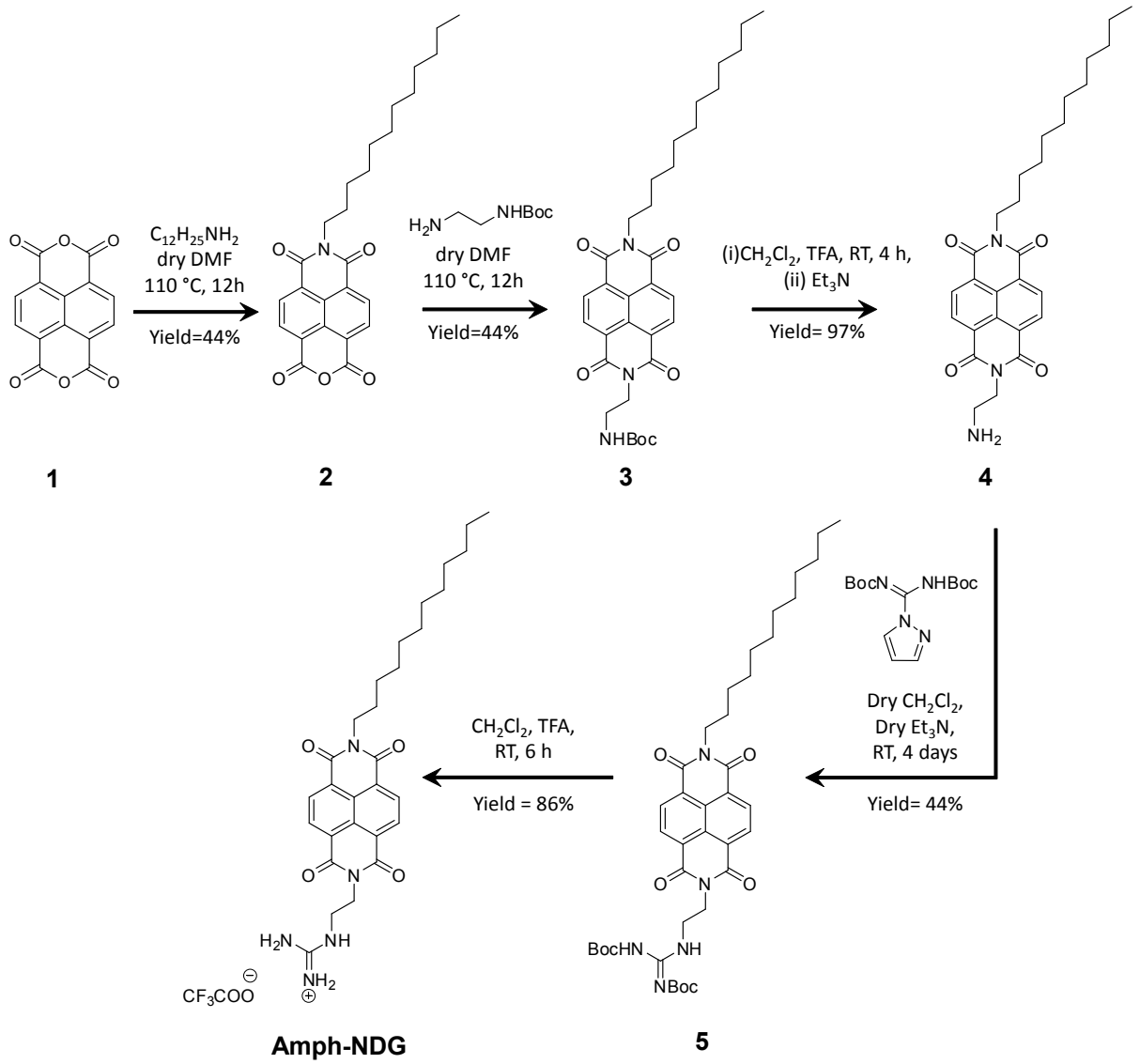

Scheme S1. Synthetic scheme for **Amph-NDG**.

Synthesis of 2: To a continuously stirred solution of 1,4,5,8-Naphthalenetetracarboxylic dianhydride (**1**) (1.00 g, 3.35 mmol) in 30 mL of dry DMF, dodecylamine (0.56 g, 3.02 mmol) dissolved in 40 mL of dry DMF was added drop wise over a period of 30 min. The reaction was carried out for 12 h under nitrogen atmosphere. After the completion of the reaction, 100 mL of H_2O was added to the reaction mixture causing precipitation of the compound

which was filtered out. The precipitate was re-dissolved in 100 mL of $CHCl_3$, and the $CHCl_3$ layer was extracted with (3 x 100 mL) of H_2O and organic layer was evaporated to give the crude product. The crude product was further purified through a flash column chromatography on silica with hexane/CH_2Cl_2 (40/60, (*v*/*v*)) eluent to give **2** as pure product.

Yield 1.11g, 44%

^{1}H NMR (400 MHz, $CDCl_3$, TMS): δ ppm 8.81 (s, 4H), 4.2 (t, *J* = 7.6 Hz, 2H), 1.75 (quin, *J* = 7.72Hz, 2H), 1.48 - 1.2 (m, 18H), 0.88 (t, *J* = 6.7 Hz, 3H).

^{13}C NMR (100 MHz, $CDCl_3$, TMS): δ ppm 162.35, 158.99, 133.29, 131.35, 129.03, 128.11, 127.01, 122.97, 77.37, 41.38, 32.06, 29.77, 29.76, 29.72, 29.65, 29.48, 29.44, 28.18, 27.21, 22.83, 14.25.

GC-MS (EI) m/z: calcd for $C_{26}H_{29}NO_5$: 435.2046, found: 435 $[M]^{+\cdot}$.

Synthesis of 3: To a solution of **2** (435 mg, 0.9 mmol) in 25 mL of dry DMF, tert-butyloxycarbonyl (Boc) protected ethylene diamine (160 mg, 1.1 mmol) dissolved in 5 mL of dry DMF was injected and the reaction mixture was stirred for 15 h under nitrogen atmosphere. After completion of the reaction, the crude product was dissolved in 100 mL of $CHCl_3$ and extracted by (3 x 100 mL) of H_2O. Then the organic layer was evaporated and the product got was purified through a flash column on silica with MeOH/CH_2Cl_2 (2/98, (*v*/*v*)) to get the pure product.

Yield 450 mg, 86%

^{1}H NMR (400 MHz, $CDCl_3$, TMS): δ ppm 8.76 (d, *J* = 0.4 Hz, 4H), 4.38 (t, *J* = 5.6 Hz, 2H), 4.19 (t, *J* = 7.7 Hz, 2H), 3.56 (q, *J* = 4.84 Hz, 2H), 1.74 (quin, *J* = 7.4 Hz, 2H), 1.45-1.2 (m, 27H), 0.87 (t, *J* = 6.7 Hz, 3H).

^{13}C NMR (100 MHz, $CDCl_3$, TMS): δ ppm 165.94, 157.34, 140.78, 135.90, 123.87, 70.56, 43.90, 42.98, 32.76, 30.34, 30.05, 29.45, 28.56, 27.45, 23.16, 14.05.

GC-MS (EI) m/z: calcd for $C_{33}H_{43}N_3O_6$: 577.3152, found: 477 $[M\text{-Boc}]^{+\cdot}$.

Synthesis of 4: To a solution of **3** (450 mg, 0.78 mmol) in CH_2Cl_2 (15 mL), TFA was added (3 mL, 38.9 mmol) and the resulting solution was stirred at room temperature for 6 h. On completion of the reaction, CH_2Cl_2 and TFA were evaporated. 10 mL of Et_3N was added to the residue and a $CHCl_3$/H_2O extraction was carried out to bring the compound to the organic layer. Finally the organic layer was evaporated to give the pure product.

Yield 360 mg, 97 %

^{1}H NMR (400 MHz, $CDCl_3$, TMS): δ ppm 8.76 (s, 4H), 4.31 (t, *J* = 6.56 Hz, 2H), 4.19 (t, *J* = 7.7 Hz, 2H), 3.10 (t, *J* = 6.6 Hz, 2H), 1.74 (quin, *J* =7.4 Hz, 2H), 1.47-1.2 (m, 18H), 0.87 (t, *J* = 6.8, 3H).

^{13}C NMR (100 MHz, $CDCl_3$, TMS): δ ppm 163.34, 162.95, 131.22, 131.07, 126.93, 126.65, 126.86, 77.36, 43.49, 41.18, 40.49, 30.06, 29.78, 29.76, 29.73, 29.67, 29.48, 28.24, 27.24, 22.84, 14.25.

GC-MS (EI) m/z: calcd for $C_{28}H_{35}N_3O_4$: 477.2628, found: 477 $[M]^{+\cdot}$.

Synthesis of 5: To a mixture of **4** (360 mg, 0.75 mmol) and diBoc protected 1H-pyrazole-1-carboxamidine (784 mg, 2.25 mmol), dry CH_2Cl_2 (20 mL) and dry Et_3N (0.8 mL, 2.25 mmol) was injected and the reaction was stirred at room temperature for 4 days. After completion of reaction, the solvent was evaporated to give the crude product. The crude product was purified by column chromatography on silica by MeOH/$CHCl_3$ (2/98 (*v*/*v*)) to give the pure product.

Yield 263 mg, 44 %

^{1}H NMR (400 MHz, $CDCl_3$, TMS): δ ppm 11.39 (s, 1H), 8.76 (s, 4H), 8.55 (t, *J* = 5.7 Hz, 1H), 4.48 (t, *J* = 5.6 Hz, 2H), 4.19 (t, *J* =7.6 Hz, 2H), 3.85 (q, *J* = 5.62 Hz, 2H), 1.74 (quin, *J* = 7.5 Hz, 2H), 1.47-1.25 (m, 36H), 0.89 (t, *J* = 6.82 Hz, 3H).

^{13}C NMR (100 MHz, $CDCl_3$, TMS): δ ppm 163.34, 163.05, 162.78, 156.72, 153.06, 131.02, 130.90, 126.84, 126.73, 126.51, 83.09, 78.91, 40.98, 39.95, 31.90, 29.62, 29.60, 29.57, 29.52, 29.32, 28.07, 28.02, 27.06, 22.67, 14.09.

HR-MS (ESI) m/z: calcd for $C_{39}H_{53}N_5O_8$: 719.3894, $[M]^+$, found: 720.3968 $[M+H]^+$.

Synthesis of Amph-NDG: To a solution of **5** (250 mg, 0.35 mmol) in CH_2Cl_2 (10 mL), TFA (2 mL, 17.36 mmol) dissolved in 5 mL of CH_2Cl_2 was added at 0 °C, and the resulting solution was stirred at room temperature for 6 h. On completion of the reaction, CH_2Cl_2 and TFA were evaporated to give a sticky solid. 50 mL of diethyl ether was added to it which caused the precipitation of the product. The solid was filtered out and dissolved in 5 mL of THF. 50 mL of diethyl ether was added to the resulting solution causing precipitation of the pure product. It was dried under vacuum to give a pale white powder.

Yield 190 mg, 86%

^{1}H NMR (400 MHz, DMSO-D_6, TMS): δ ppm 8.70 (d, *J* = 1.16 Hz, 4H), 7.47 (t, *J* = 6.36 Hz, 1H), 7.3-6.96 (br s, 3H), 4.22 (t, *J* = 5.28 Hz, 2H), 4.06 (t, *J* = 7.46 Hz, 2H), 3.52 (q, *J* = 5.72 Hz, 2H), 1.66 (quin, *J* = 7.3 Hz, 2H), 1.42-1.18 (m, 20 H), 0.85 (t, *J* = 6.8 Hz, 3H).

^{13}C NMR (100 MHz, DMSO-D_6, TMS): δ ppm 162.90, 162.54, 156.93, 130.40, 126.33, 126.29, 126.21, 126.11, 31.23, 28.96, 28.92, 28.82, 28.63, 27.31, 26.43, 22.02, 13.88.

HR-MS (ESI) m/z: calcd for $C_{31}H_{38}F_3N_5O_6$: 633.2774, $[M]^+$, found: 520.2918 $[M\text{-}CF_3COO^-]^+$.

MALDI m/z: calcd for $C_{31}H_{38}F_3N_5O_6$: 633.2774, $[M]^+$, found: 520.30 $[M\text{-}CF_3COO^-]^+$.

3. Experimental Procedures

3.1 Protocol of sample preparation:

Spectroscopic grade solvents from commercial sources and distilled water were used for performing all the studies at room temperature. Stocks of **Amph-NDG** were prepared as 10^{-3} M in THF and stocks of ATP were prepared in 10 mM solution of HEPES buffer. All solutions were prepared by injecting a monomeric solution of **Amph-NDG** in THF to ATP containing HEPES to make a total volume of 2.5 mL and achieve the desired concentration of the solution to be measured and the time dependent growth was monitored. The desired temperature was maintained throughout the measurements. All the measurements were started immediately after all the required components are added.

3.2 Quantum Calculations:

The structures are optimized using Gaussian and plane waves (GPW) method, the gaussians are mapped onto five grid levels and the planewave cut-off is set to be 280 Ry, which was implemented in QUICKSTEP[S1] a part of CP2K package.[S2] The exchange-correlation potential was treated with the generalized gradient approximation parameterized by the spin-polarized Perdew-Burke-Ernzerhof functional (PBE).[S3] The Goedecker-Teter-Hutter (GTH) pseudopotentials[S4,S5] are used to represent the effective potential from core electrons of an atom along with its nucleus. The dispersion corrections are taken care by the Grimme[S6] DFT-D3 method. DZVP-MOLOPT-SRGTH basis set is used to represent the electronic wave function in the density-functional theory (DFT). The preformed trimer was kept in an orthogonal box of dimensions 30, 50, 40 Å and the stacks are oriented along Z-axis.

Construction and Geometry Optimization of bilayer 18-mer:

The construction of an 18-mer is made in the following steps:

1. The preformed trimer was taken as a preliminary unit in the construction bilayer 18-mer. The preformed trimer constructed in such a way that the stacking axis is parallel to Z-axis.

2. A bilayer trimer was constructed from a preformed trimer and its image, the image was formed by rotating the trimer to 180± around the stacking axis (Z-axis) and by translation in XY-plane by vector -1.0, 10.0, 0.0 Å.

3. The bilayer trimer was a template for bilayer construction. The bilayer 18-mer was constructed by replicating the bilayer trimer unit with a twist angle of 6± along with a translation of 11.7 Å in Z-direction. Finally, the bilayer 18-mer has 36 monomers of NDG and 12 ATP molecules. The preformed bilayer 18-mer in a cubic box of size 100 Å was optimized using a semi-empirical quantum method, PM6[S7] in CP2K package in gas-phase.

3.3 Kinetic fitting of nucleation growth for different equiv. of ATP:

The normalized absorbance nucleation growth kinetics was fitted to a 2-step model proposed by Watzky and Finke [S8] and the following equation has been used to fit the data:

$$B = \frac{A_o - \dfrac{\dfrac{k_n}{k_e} + A_o}{1 + \dfrac{k_n}{k_e A_o} e^{(k_n + k_e A_o)t}}}{A_o} \qquad 1$$

A_o is the concentration of the monomeric species, B is the concentration of the elongating species growing exponentially, k_n is the rate of nucleation and k_e is the rate of growth.

4. Supporting Figures

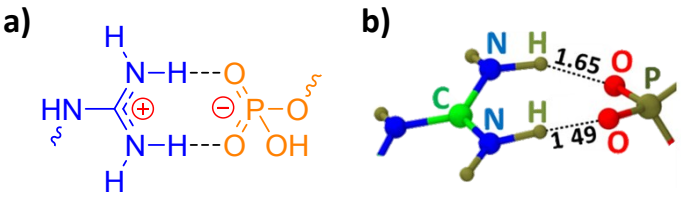

Figure S1. Salt-bridge interactions. a) Molecular representation and b) representation by quantum optimizations at M06-2X/6-311g level of theory using Gaussian package[S9] for salt-bridge interaction between cationic guanidinium and anionic phosphate. Guanidinium is abundantly found in naturally occurring proteins and is known to interact with oxyanions

such as phosphates through salt-bridge like interactions. The salt-bridge interaction is formed via a combination of electrostatic and hydrogen bonds.[S10] The O-H bond distance has been mentioned in black over the dotted line.

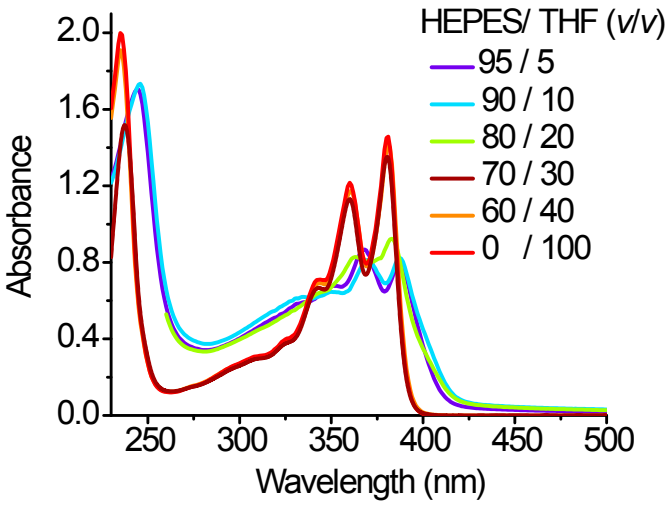

Figure S2. Effect of varying solvent composition on Amph-NDG self-assembly. UV-Vis absorption spectral changes of **Amph-NDG** in the absence of ATP with varying HEPES and THF composition ([**Amph-NDG**] = 5 x 10^{-5} M, 25 °C).

Note: The molecule itself self-assembles owing to its amphiphilic design at a higher percentage of H_2O (>HEPES/THF, 70/30, (*v*/*v*)) as seen from the broadened absorption spectra but exists in a molecularly dissolved state at a lower percentage of H_2O.

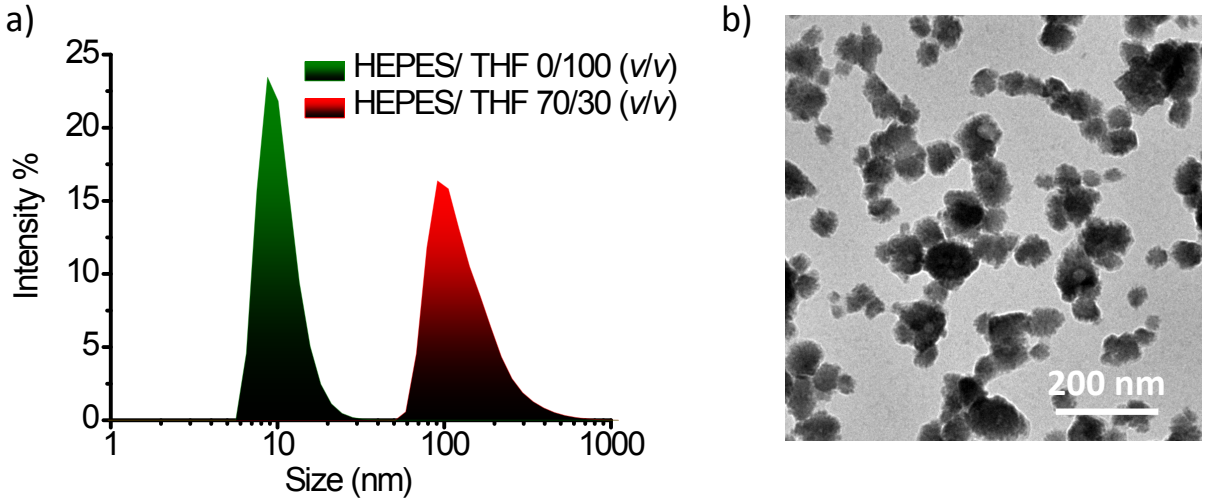

Figure S3. Effect of varying solvent composition on Amph-NDG self-assembly. a) DLS spectra of **Amph-NDG** showing increase in size on changing the solvent composition (HEPES/THF, 70/30 (*v*/*v*)). b) TEM images (stained with uranyl acetate, 1 wt. % in water) of **Amph-NDG** in H_2O/THF, 70/30, (*v*/*v*) solvent mixture ([**Amph-NDG**] = 5 x 10^{-5} M, 25 °C).

Note: Amph-NDG molecules exist in a molecularly dissolved state in THF and self-assemble into small undefined aggregates in HEPES/THF (70/30 (*v*/*v*)) due to their amphiphilic design in a water-rich solvent system.

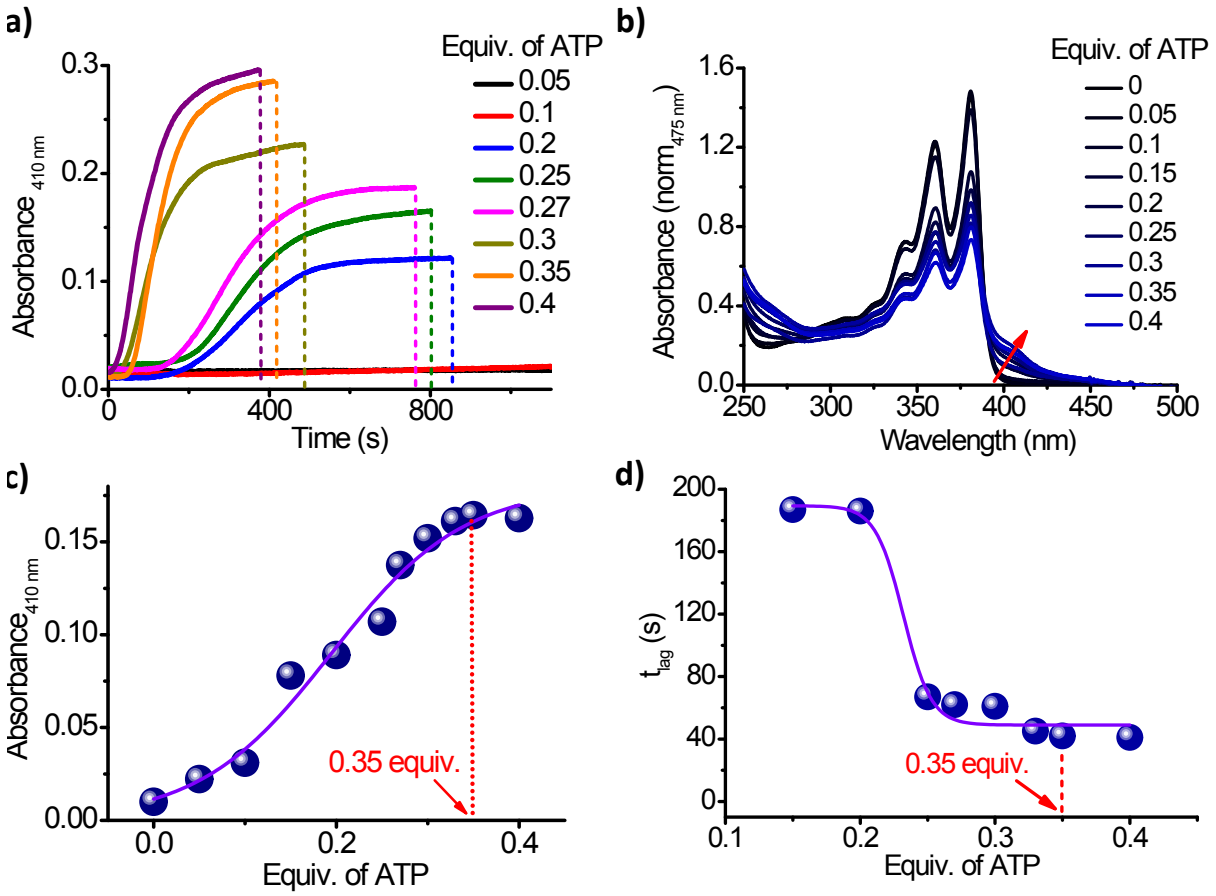

Figure S4. Fuel dependence on the nucleation-growth. a) Time dependant UV-Vis absorption changes monitored at λ= 410 nm, b) final absorption spectra after the completion of growth, c) ATP titration curve obtained from absorption spectra at λ= 410 nm and d) lag time (t_{lag}) for varying equiv. of ATP. ([**Amph-NDG**] = 5 x 10^{-5} M, HEPES/ THF, 70/30, (*v*/*v*), 25 °C).

Note: The titration curve constructed by taking the absorbance values at λ = 410 nm (aggregate band), obtained from the normalized absorption spectra after complete growth, showed that the binding sites on **Amph-NDG** saturates around 0.35 equivalents (equiv.) of ATP. With increasing equiv. of ATP, we observed a decrease in t_{lag} which also saturates around 0.35 equiv. of ATP. Hence 0.35 equiv. of ATP was used throughout the present study.

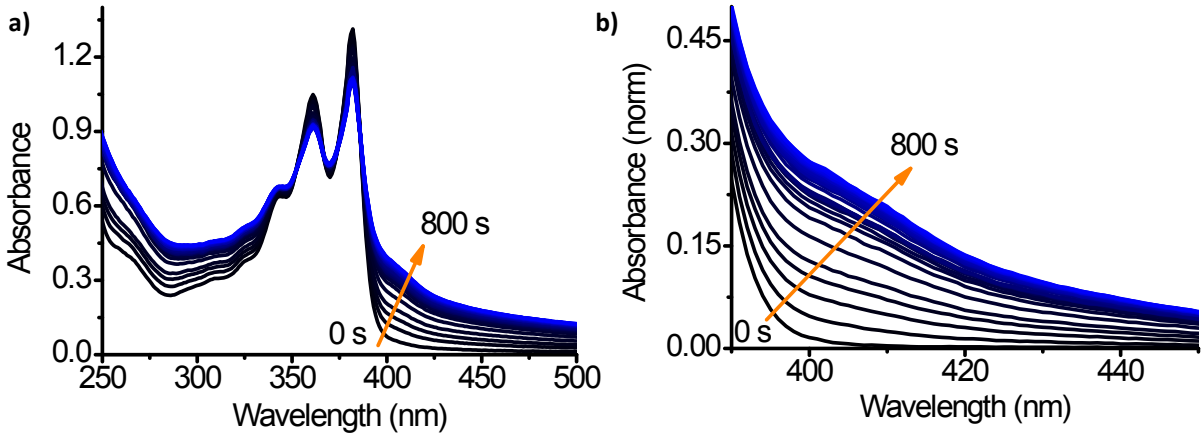

Figure S5. Absorption spectral changes on ATP driven self-assembly of Amph-NDG. Time dependent a) UV-Vis absorption a) zoomed (normalised) UV-Vis absorption changes of **Amph-NDG** upon ATP binding (rate = 500 nm/min). (c = 5 x 10^{-5} M, with 0.35 equiv. of ATP, HEPES/THF, 70/30, (*v*/*v*), 25 °C).

The emergence of aggregate band at λ = 410 nm over time when ATP induces self-assembly of **Amph-NDG** is more pronounced in normalised absorption spectra.

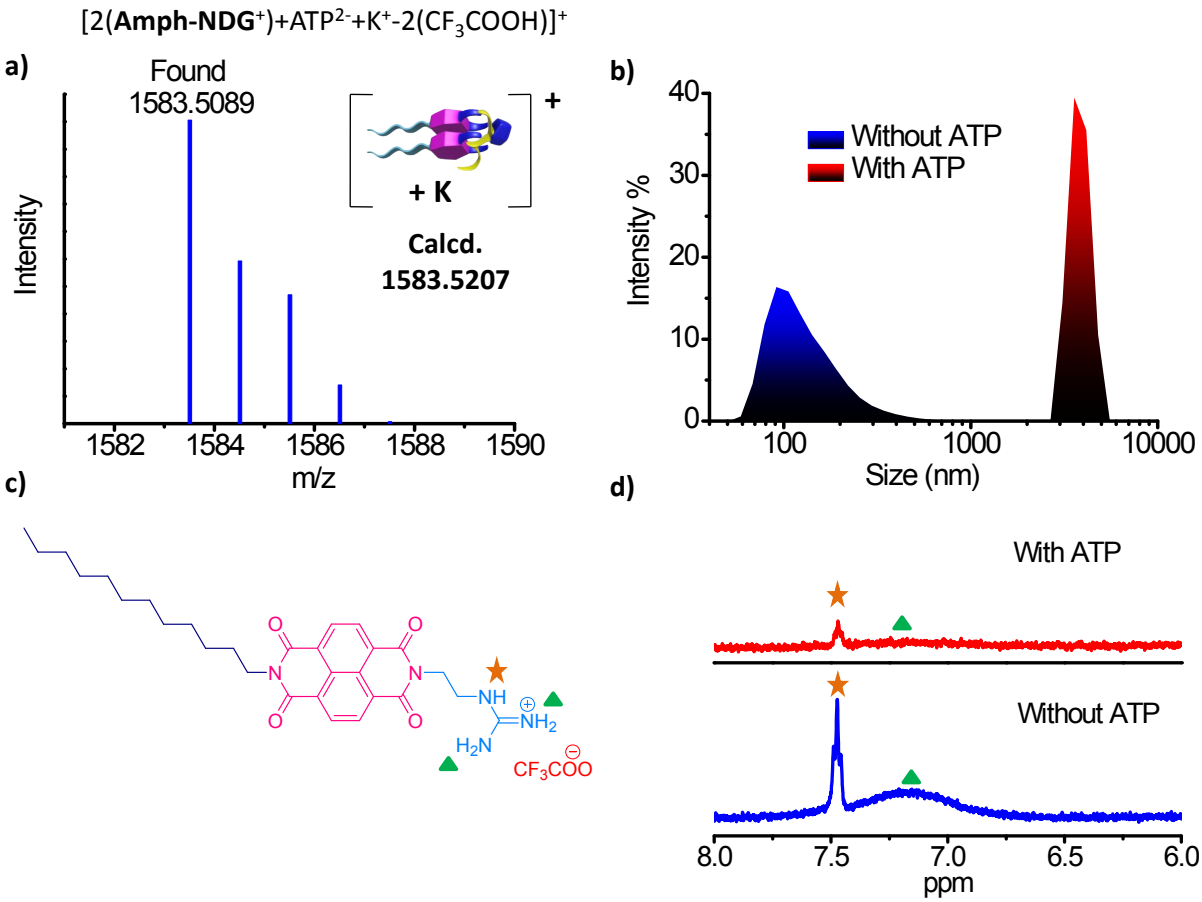

Figure S6. ATP-driven self-assembly of Amph-NDG. a) High-resolution ESI-MS spectrum giving the mass of two molecules of **Amph-NDG** bound to one molecule of ATP([**Amph-NDG**] = 10^{-3} M). The m/z = 1583.5089 (+1) corresponds to [2(**Amph-NDG**$^{+}$) + ATP^{2-} + K^{+} - 2(CF_3COOH)]$^{+}$ whereas the expected value is m/z = 1583.5207. Schematic in the inset represents the corresponding clipped complex. b) DLS spectra showing increase in size after complete growth process of ATP bound **Amph-NDG** ([**Amph-NDG**] = 5 x 10^{-5} M, HEPES/ THF, 70/30 (*v*/*v*), with 0.35 equiv. of ATP). c) Molecular structure of **Amph-NDG** with marked protons of interest. d) ^{1}HNMR of **Amph-NDG** with (red) and without (blue) ATP showing that H-bonded protons broaden out due to aggregation (100% DMSO-D_6) ([**Amph-NDG**] = 10^{-3} M, 25 °C). These results confirm the formation of ATP binding induced self-assembly of **Amph-NDG**.

Spectroscopic Probe	t_{lag} (s)	t_{50} (s)	t_m (s)	v_{max} (s^{-1})	t_e (s)
UV-Vis Absorbance	62 ± 2	118 ± 2	89 ± 2	$8.76x10^{-3} \pm 1.68x10^{-4}$	419 ± 2
CD	90 ± 3	139 ± 3	107 ± 3	$7.89x10^{-3} \pm 0.39x10^{-4}$	405 ± 3

Table S1. Calculated time parameters of the nucleation-growth measured via various spectroscopic tools. t_{lag} and t_{50} (half-time i.e. time required for completion of 50% of the process) from tangent drawn at the inflection point t_m (time at which growth rate reaches its maximum i.e. v_{max})[S11] and t_e (total time for completion of growth) could be calculated. ([**Amph-NDG**] = 5 x 10^{-5} M, HEPES/ THF, 70/30 (*v*/*v*), with 0.35 equiv. of ATP, 25 °C).

Equiv. of ATP	t_{lag} (s)	t_{50} (s)	t_m (s)	v_{max} (s^{-1})	t_e (s)
0.15	187 ± 4	339 ± 4	322 ± 4	$3.28\ x10^{-3} \pm 3.64x10^{-4}$	855± 4
0.2	186 ± 2	338 ± 2	302 ± 2	$3.24\ x10^{-3} \pm 2.33x10^{-4}$	802± 2
0.25	167 ± 2	299 ± 2	276 ± 2	$3.79x10^{-3} \pm 2.32x10^{-4}$	763± 2
0.3	71 ± 1	134 ± 1	85 ± 1	$7.62x10^{-3} \pm 1.61x10^{-4}$	457± 1
0.33	68 ± 3	123 ± 3	83 ± 3	$6.25x10^{-3} \pm 2.41x10^{-4}$	420± 3
0.35	62 ± 2	118 ± 2	89 ± 2	$8.76x10^{-3} \pm 1.68x10^{-4}$	417 ± 2
0.38	61 ± 1	123 ± 1	91 ± 1	$7.19x10^{-3} \pm 2.41x10^{-4}$	407± 1
0.4	45 ± 3	108 ± 3	83 ± 3	$6.73x10^{-3} \pm 1.81x10^{-4}$	391± 3

Table S2. Calculated time parameters of the growth measured via UV-Vis absorption measurements. With an increase in equiv. of ATP there is a decrease in all the calculated time parameters while v_{max} increases. These values also saturate around 0.35 equiv. of ATP ([**Amph-NDG**] = 5 x 10^{-5} M, HEPES/ THF, 70/30, (*v*/*v*), 25 °C).

Equiv. of ATP	A_o (x 10^{-5} M)	k_n (x10^{-3} min^{-1})	k_e (M^{-1} min^{-1})	Adj. R^2
0.15	5	0.62	141.9	> 0.99
0.2	5	1.31	191.45	> 0.99
0.25	5	1.51	228.2	> 0.99
0.3	5	1.88	207.51	> 0.99
0.33	5	5.35	236.21	> 0.99
0.35	5	5.21	319.84	> 0.99
0.38	5	5.73	326.07	> 0.99
0.4	5	5.75	391.23	> 0.99

Table S3. Parameters got from the fitting of kinetic data in Figure S4. Various parameters derived from the curves fitted to equation 1 for different equiv. of ATP. There is an increase in k_n as well as k_e with increasing equiv. of ATP which saturates around 0.35 equiv. of ATP. ([**Amph-NDG**] = 5 x 10^{-5} M, HEPES/ THF, 70/30, (*v*/*v*), 25 °C).

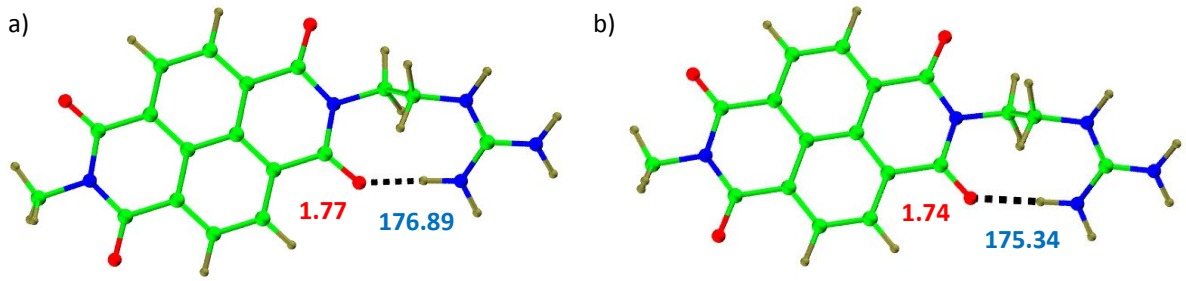

Figure S7. Optimization of Amph-NDG in quantum calculations at M06-2x/6-311g level of theory using Gaussian package.[S9] a) Initial and b) final configuration of **Amph-NDG** molecular structures. The black dotted lines represent the intramolecular hydrogen bond between guanidinium N-H and imide C=O. The intramolecular hydrogen bond distance is shown in red and the O-H-N (acceptor-hydrogen-donor) angle is shown in blue. The dodecyl chain has been replaced by methyl group for geometry optimization to decrease computational cost.

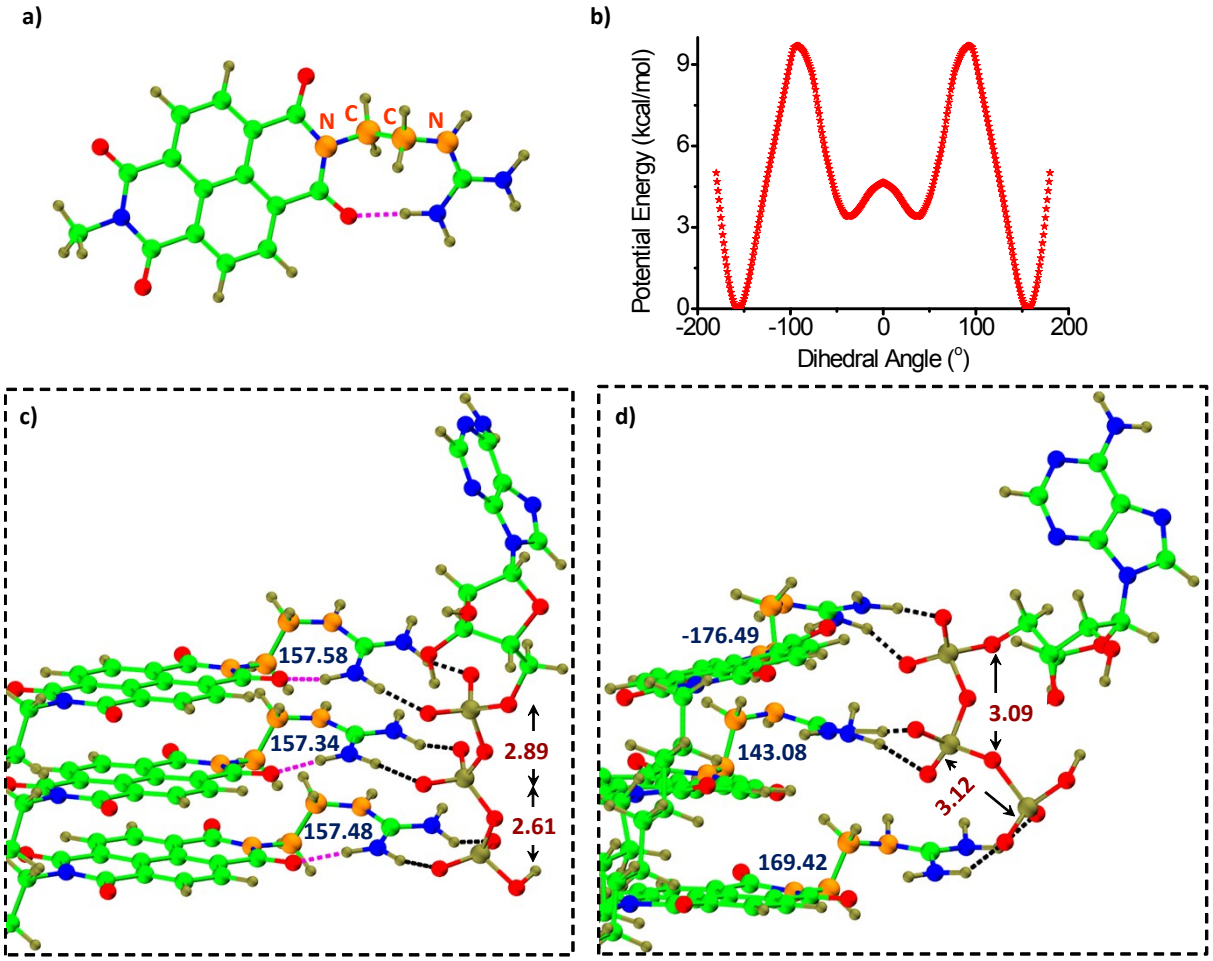

Figure S8. Potential Energy Surface Scan for N-C-C-N dihedral angle. a) Optimized monomer unit of **Amph-NDG,** wherein the dodecyl chain has been replaced by a methyl group for geometry optimization. b) Potential energy surface scan showing the potential surface for the N-C-C-N dihedral angle in gas-phase at M06-2X/6-311g level of theory using Gaussian package.[S9] Zoomed portion of ATP bound trimer of **Amph-NDG** configuration at c) initial and d) final stage. The intramolecular and intermolecular hydrogen bonds are shown in magenta and black dotted lines, respectively. The intramolecular hydrogen bond is between N-H of guanidinium and C=O of imide and the intermolecular hydrogen bonds are between the phosphate of ATP and guanidinium of **Amph-NDG** molecule. Phosphate-phosphate distance is shown in maroon colour and the dihedral angle is shown in blue colour and the N-C-C-N atoms forming the dihedral angle are highlighted in orange.

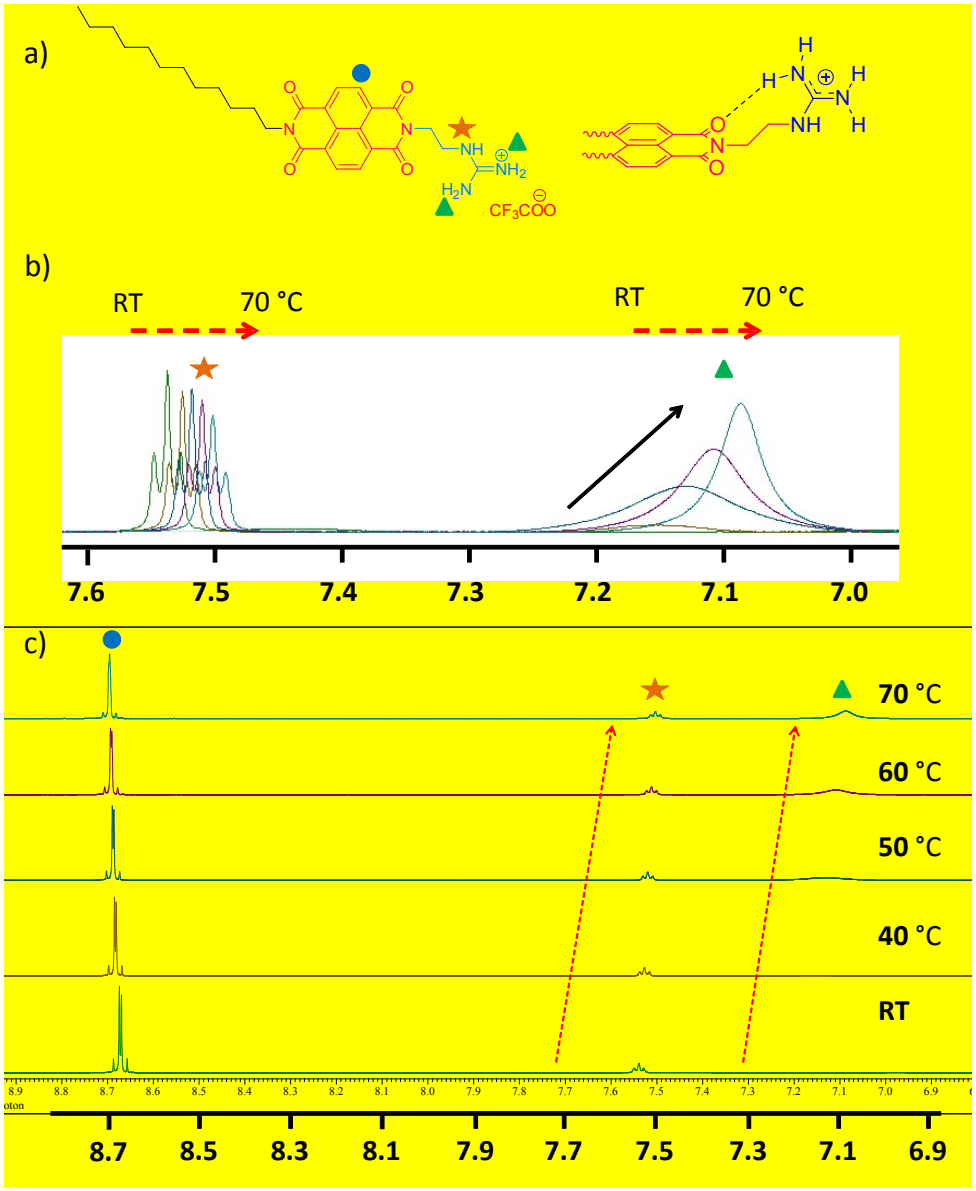

Figure S9. NMR changes of Amph-NDG with temperature. a) Molecular structure of **Amph-NDG** where the protons of interest are marked. Intramolecular hydrogen bond between guanidinium N-H and imide C=O has been shown. b) Overlaid and c) separated VT (variable temperature) ^{1}H NMR of **Amph-NDG**. ([**Amph-NDG**] = 10^{-3} M, DMSO-D_6, 25 °C to 70 °C).

Note: The hydrogen bond exists between guanidinium N-H and imide C=O which has been proven by an upfield shift as well as an increase in intensity for the N-H of intramolecularly hydrogen-bonded guandinium group of molecularly dissolved **Amph-NDG** with increase in temperature. We expect a similar re-arrangement during the ATP-driven assembly of **Amph-NDG** in HEPES/THF, 70/30, (*v*/*v*), which could not be studied through NMR due to stacking of chromophores in this solvent composition.

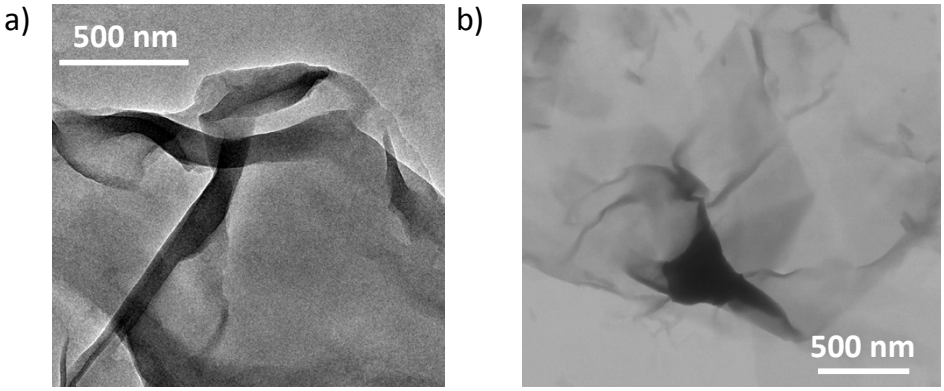

Figure S10. Morphological characterizations of ATP bound Amph-NDG. a) TEM and b) STEM image of ATP bound **Amph-NDG** after completion of the growth process showing the presence of sheets. ([**Amph-NDG**] = 5 x 10^{-5} M, with 0.35 equiv. of ATP, H_2O/THF, 70/30, (*v*/*v*), 25 °C).

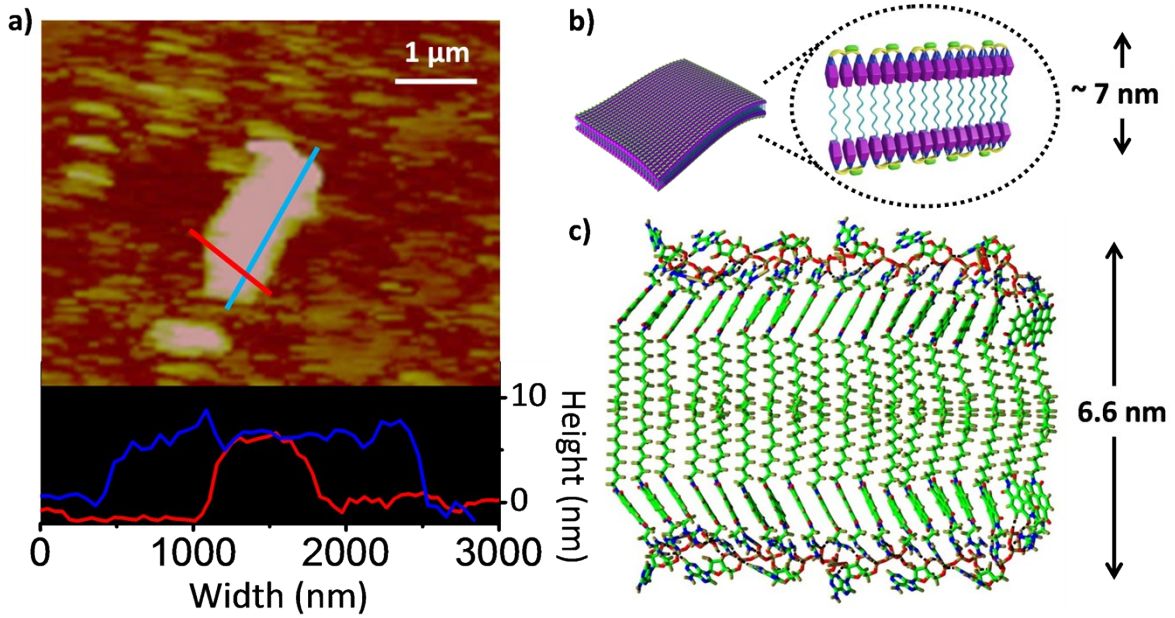

Figure S11. Bilayer distance of ATP bound Amph-NDG sheets. a) AFM image of ATP bound **Amph-NDG** after completion of growth process showing the presence of sheets ([**Amph-NDG**] = 5 x 10^{-5} M, with 0.35 equiv. of ATP, H_2O/THF, 70/30, (*v*/*v*), 25 °C). The height profile of ATP bound **Amph-NDG** from AFM corresponds to ~7 nm, which is the bilayer thickness. b) Schematic representation of the sheet morphology obtained from ATP bound **Amph-NDG** and its bilayer packing with non-interdigitated alkyl chains and c) final structure of a preformed 18-mer optimized using the semi-empirical PM6 method where the average bilayer width was found to be 6.6 nm. Such an arrangement suggests that **Amph-NDG**

molecules are arranged vertically along the thickness of the sheets with the ATP bound guanidinium exposed outside to the hydrophilic environment.

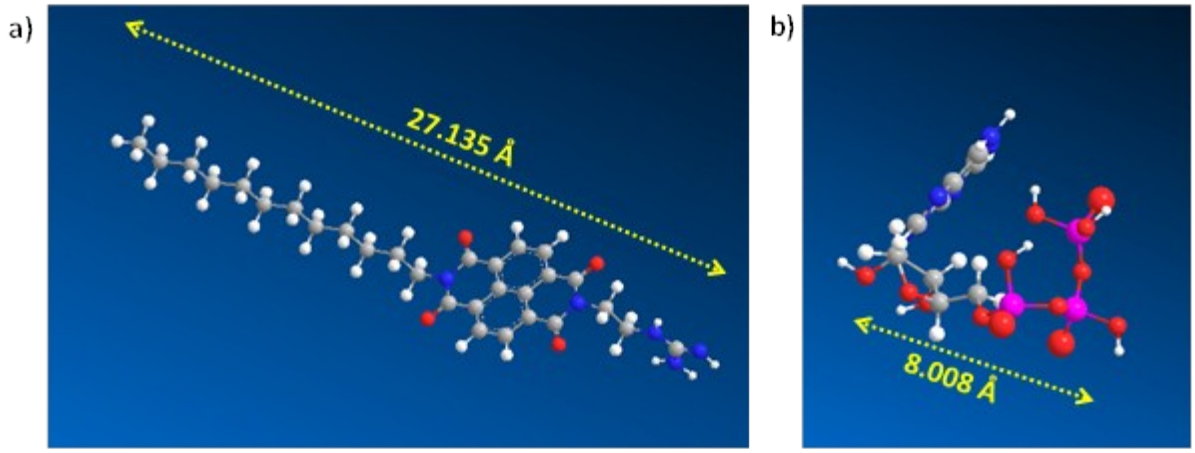

Figure S12. Minimized structures from ChemDraw. Minimized structures of a) Amph-NDg and b) ATP obtained from ChemDraw.

Note: We could confirm non-interdigitation between the alkyl chains by matching the molecular dimensions of **Amph-NDG** and ATP (2.7 nm + 0.8 nm) i.e. 3.5 nm. Hence the bilayer distance achieved from AFM is ~7 nm which is double the overall molecular dimensions. Interdigitation would have caused the bilayer distance to decrease significantly hence decreasing the height of the sheets.

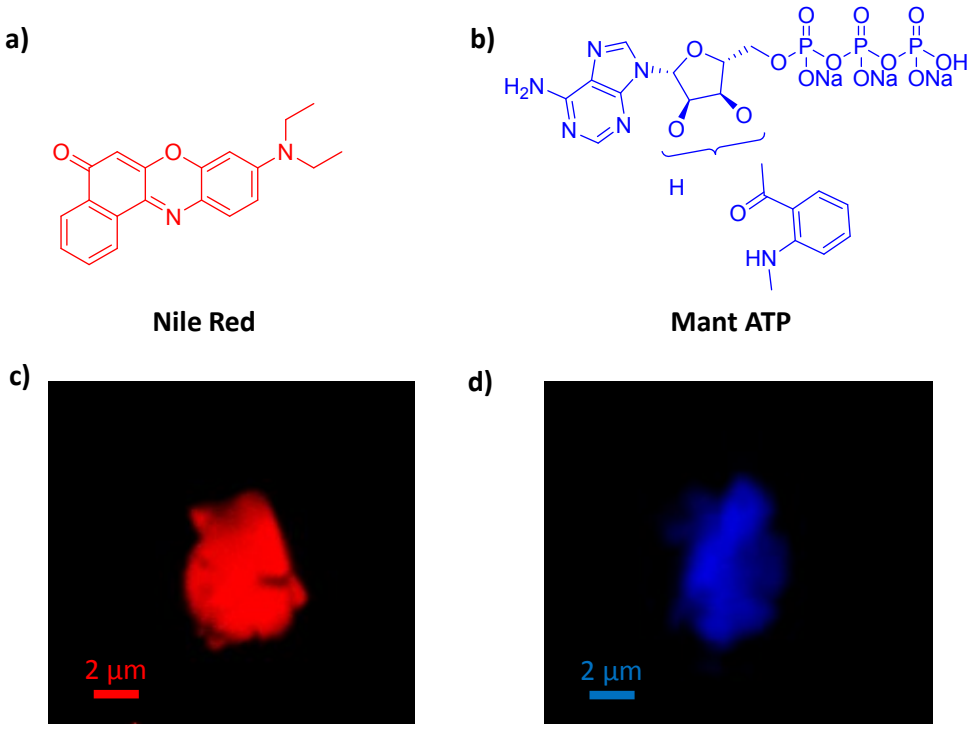

Figure S13. **Sheet structures in the solution phase.** Molecular structures of a) Nile red and b) Mant (2'-(or-3')-*O*-(*N*-Methylanthraniloyl))-ATP. Confocal images of ATP bound **Amph-NDG** sheets c) with Nile red (1 µM, λ_{ex}= 550 nm, λ_{em}= 650 nm) and d) with ATP:Mant ATP (λ_{ex}= 355 nm, λ_{em}= 488 nm) in 1:1 ratio. ([**Amph-NDG**] = 5 x 10^{-5} M, with 0.35 equiv. of ATP, H_2O/THF, 70/30, (*v*/*v*), 25 °C). Due to the hydrophobic nature of Nile red, it gets entrapped in the bilayer formed by amphiphilic **Amph-NDG** molecule. Mant-ATP (fluorescent) along with ATP (1:1) interacts with **Amph-NDG** making the sheets fluorescent.

Note: All the above morphological characterizations confirm the formation of two-dimensional sheets like structures of ATP bound **Amph-NDG** which is established by the presence of fluorescent sheets in solution phase as seen from the confocal images.

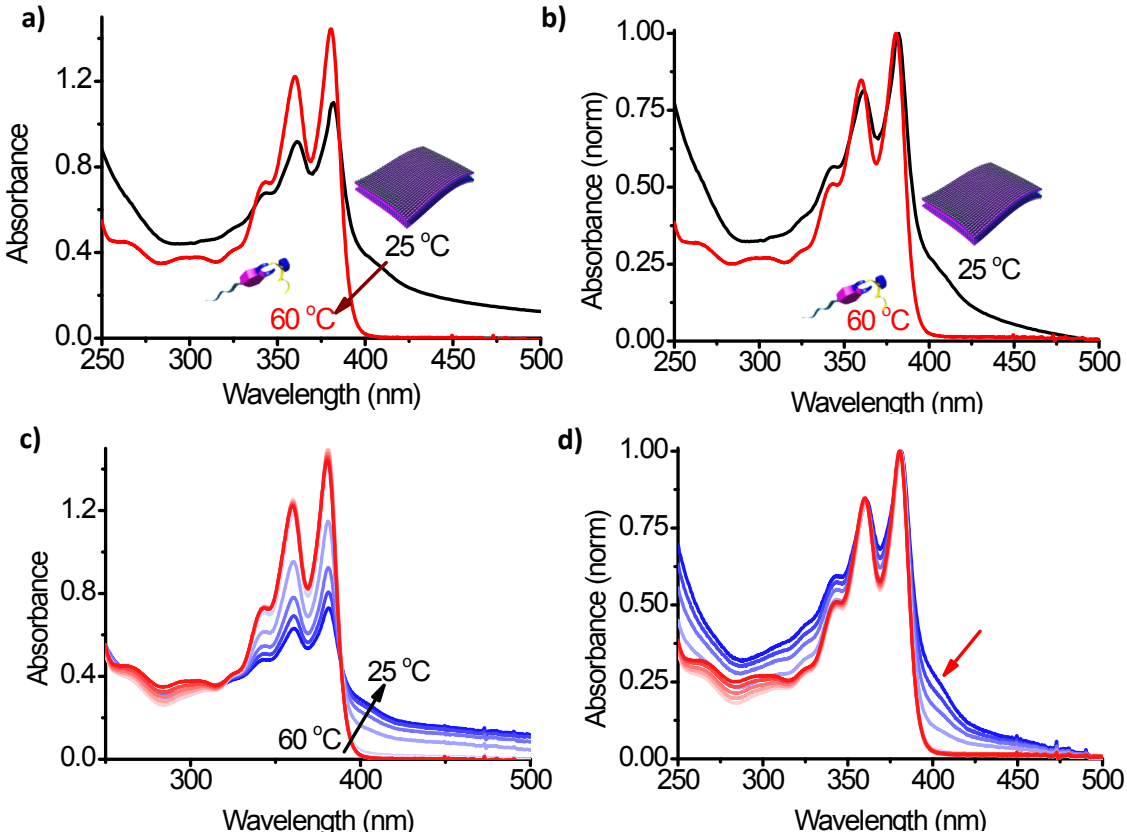

Figure S14. Effect of temperature on ATP bound Amph-NDG. Absorption spectral changes on a and b) heating from 25 °C to 60 °C with a disappearance of aggregation band at λ = 410 nm and c and d) cooling from 60 °C to 25 °C where a and c are unnormalised and b and d are normalised. Red arrow in Figure d points at the aggregate band at λ = 410. (-dT/dt = 1 °C/min) (c = 5 x 10^{-5} M, with 0.35 equiv. of ATP, HEPES/THF, 70/30, (*v*/*v*)).

Note: On heating the temporally grown solution of ATP bound **Amph-NDG** to 60 °C, the ATP bound assembly completely melts as reflected from the UV-vis absorption spectra at 60 °C where the aggregate band at λ = 410 nm completely disappears and revival of sharp absorption features occur corresponding to molecularly dissolved naphthalene diimide molecules. Consequently, when annealed from 60 °C to 25 °C, gradual broadening in absorption spectra is observed along with the emergence of aggregate band at λ= 410 nm indicating the recovery of self-assembly. These changes are more pronounced in the normalised absorption spectra.

Conc (M)	T_e (K)
10^{-4}	313.74
$9x10^{-5}$	312.8
$7.5x10^{-5}$	310.75
$5x10^{-5}$	308.33

Table S4. Elongation temperature (T_e) obtained from cooling curves. Obtained by monitoring λ= 410 nm in the absorption spectra of annealed ATP bound **Amph-NDG** for different concentrations. (-dT/dt = 1 K/min, HEPES/THF, 70/30, (*v*/*v*), with 0.35 equiv. of ATP).

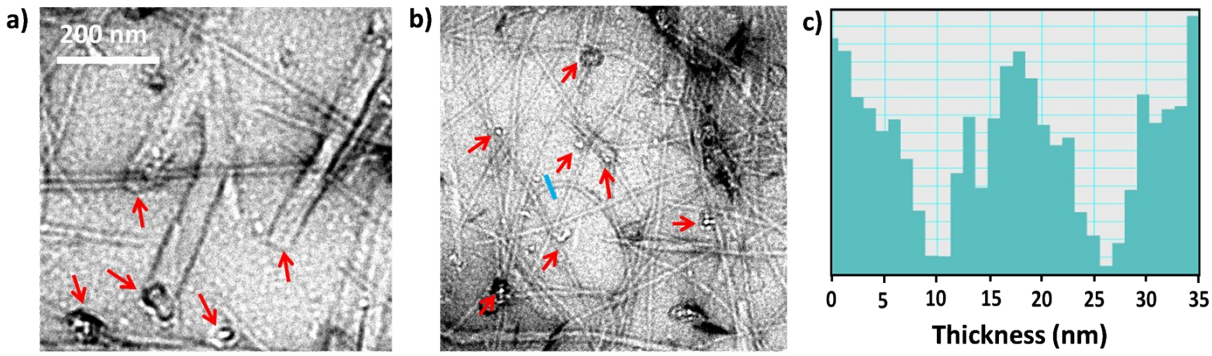

Figure S15. Morphological characterizations of annealed ATP bound Amph-NDG. a) and b) TEM images (stained with uranyl acetate, 1 wt. % in water) of ATP bound **Amph-NDG** on annealing. c) Intensity profile of the tube obtained from the blue trace of TEM image. Red arrows point towards the openings of the tubes. (-dT/dt = 1 K/min, [**Amph-NDG**] = 5 x 10^{-5} M, with 0.35 equiv. of ATP, H_2O/THF, 70/30, (*v*/*v*)). Figure a shows the presence of scrolled tubes as the intermediate morphologies.

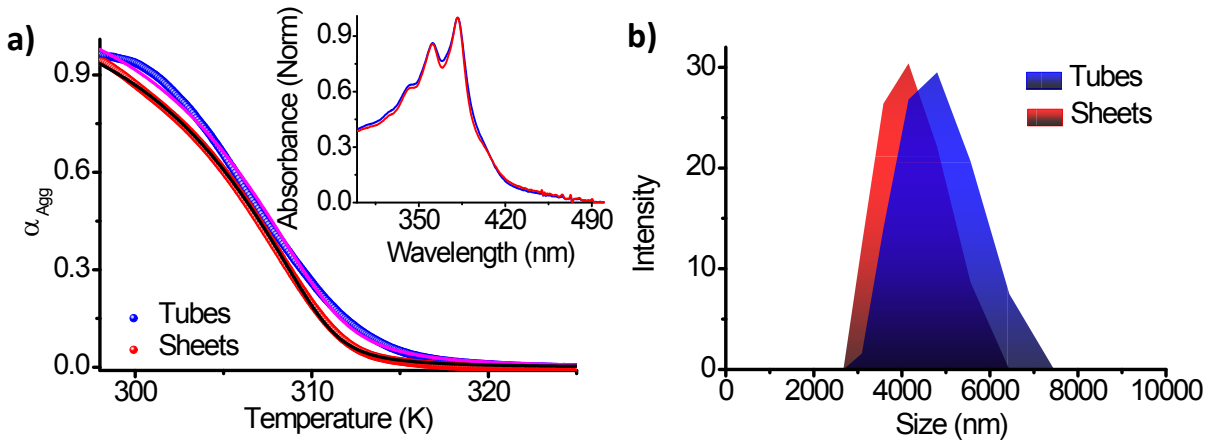

Figure S16. Difference between sheets and tubes. a) Temperature dependent degree of supramolecular polymerization (α_{Agg}) of ATP bound **Amph-NDG** for sheets and tubes obtained by melting both assemblies from 25 °C to 60 °C. Inset shows the absorption spectra obtained for sheets and tubes. b) Size obtained for temporally acquired sheets and annealed tubes of ATP bound **Amph-NDG** from DLS show a similar size for both (dT/dt = 1 K/min, HEPES/THF, 70/30, (*v/v*), 25 °C).

Note: A small change is observed in melting curves for sheets and tubes. Whereas, the absorption spectra for both sheets and tubes coincides indicating similar packing in both the assemblies.

Melting	**ΔH^{o}_{m} (kJ mol^{-1})**	**ΔS^{o}_{m} (kJ K^{-1} mol^{-1})**	**T_m (K)**	**ΔG_m (kJ mol^{-1})**
Sheet	-111.56±1.74	-0.28±0.01	309.95± 0.04	-28.12
Tube	-105.13 ± 1.18	-0.25 ± 0.005	311.21 ± 0.04	-30.63

Table S5. Thermodynamic parameters obtained from co-operative fits of melting curves. Thermodynamic parameters have been obtained by fitting the temperature dependent degree of ATP bound **Amph-NDG** aggregation to the temperature-dependent nucleation-elongation model.[S12] ΔH°_{m} refers to the enthalpy of melting, ΔS°_{m} is the entropy of melting, T_m is the melting temperature and ΔG_m refers to Gibb's free energy of melting. The T_m for tubes is a little higher than the sheets and the calculated ΔG_m value for tubes is also more than sheets indicating that the tube is thermodynamically more stable than sheet (dT/dt = 1 K/min, HEPES/THF, 70/30, (*v/v*), 25 °C).

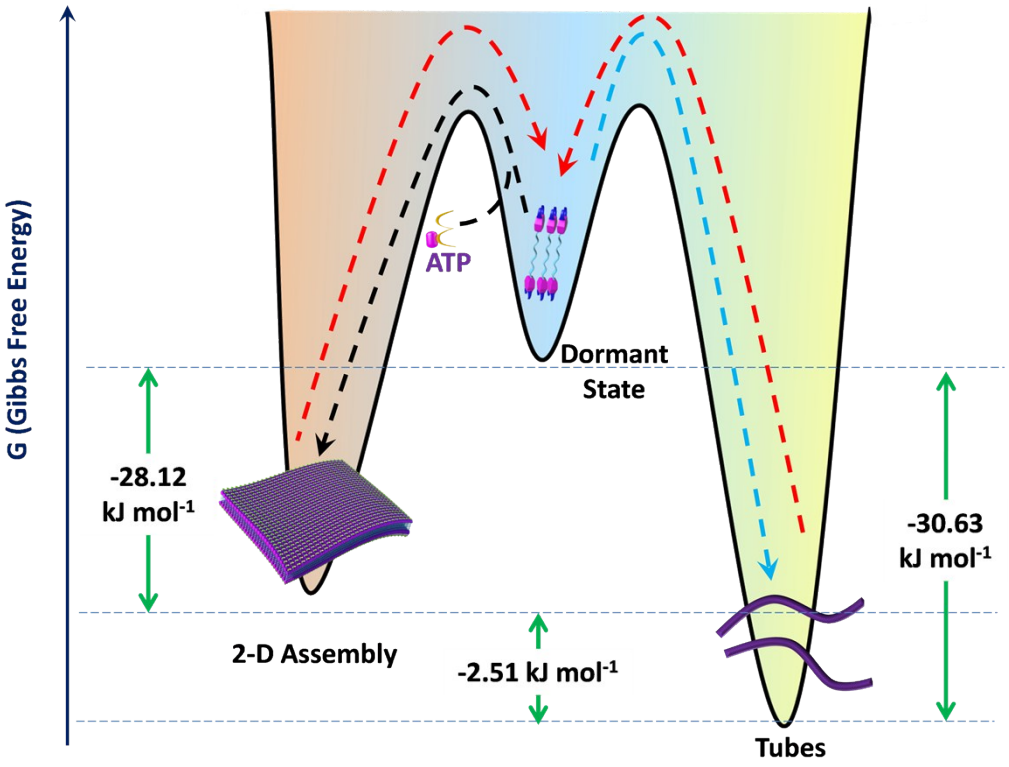

Figure S17. Schematic representation of self-assembly energy landscapes of ATP bound **Amph-NDG**. It indicates that the annealed tubes are thermodynamically more stable than temporally grown sheets.

5. Spectral Copies

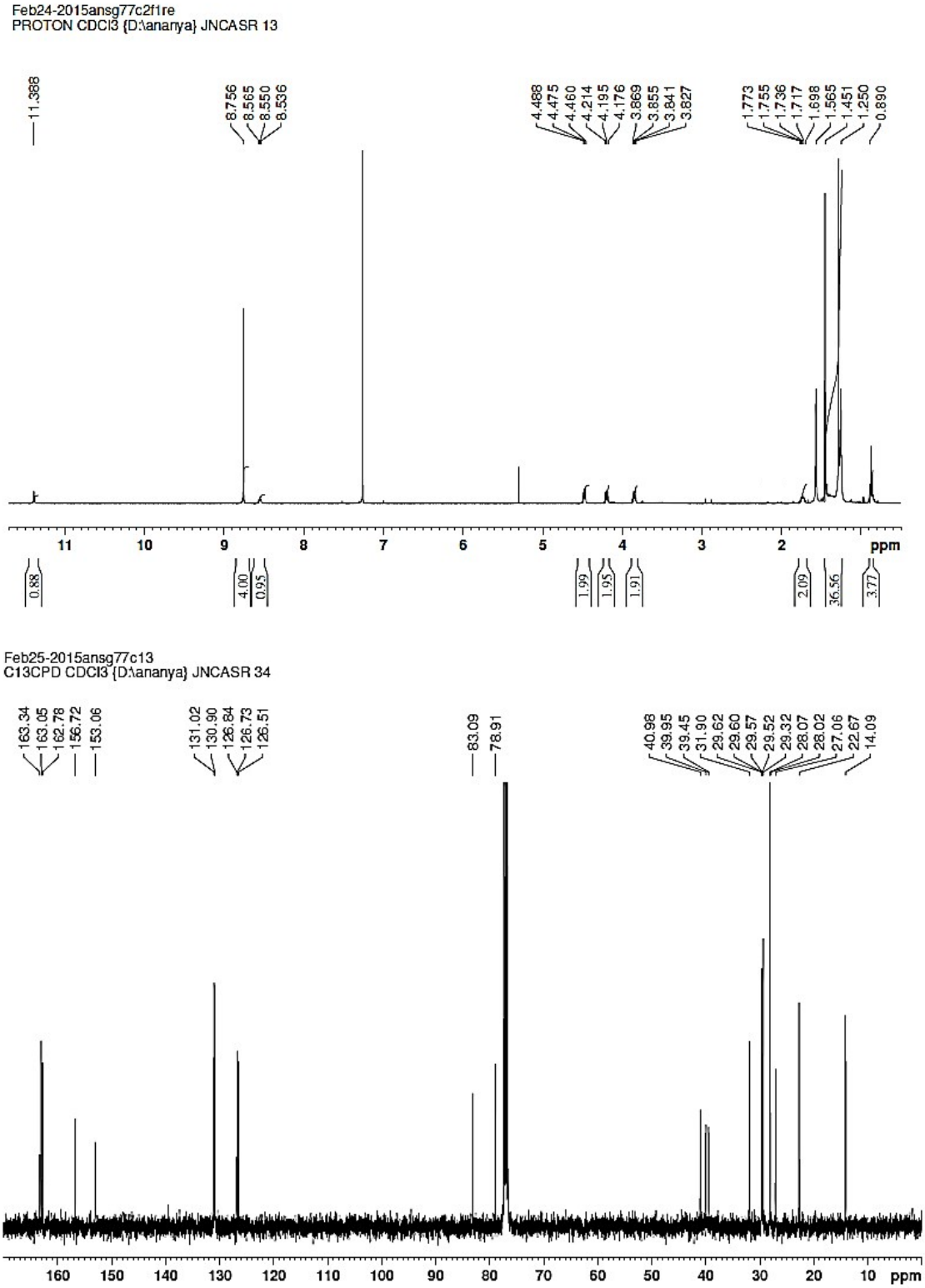

Figure S18. ^{1}H NMR and ^{13}C NMR of **5.**

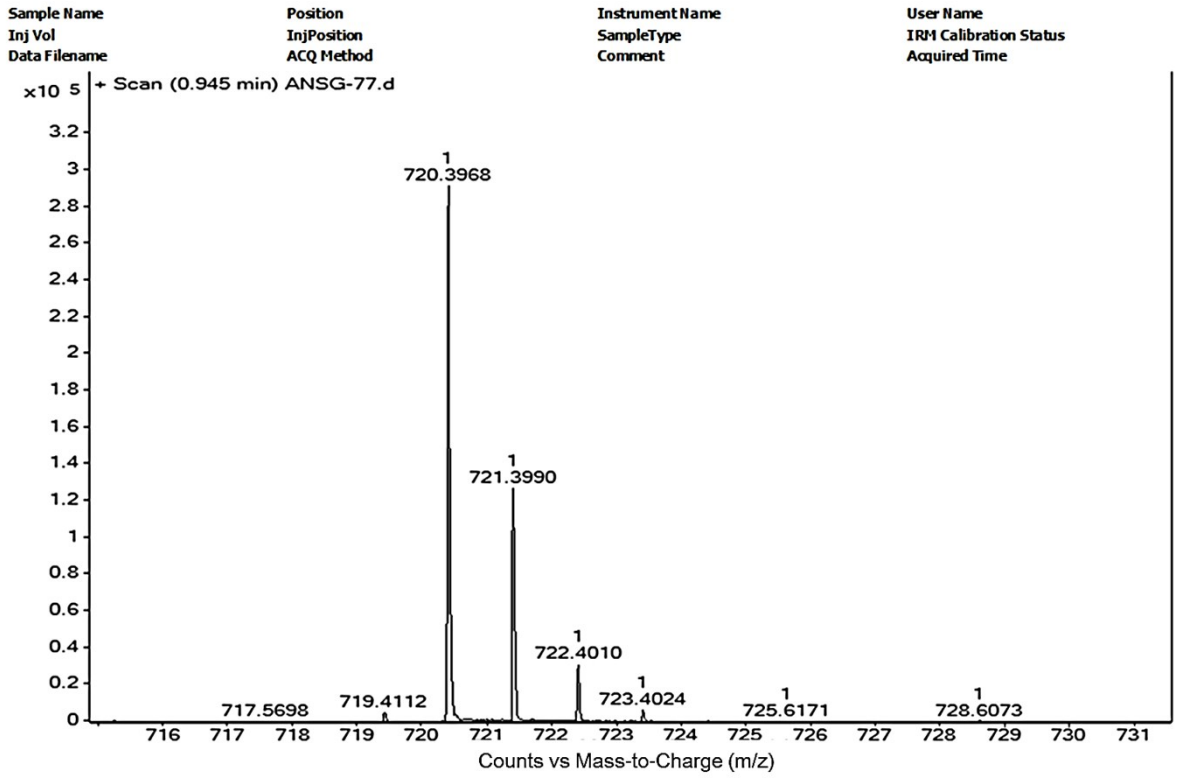

Figure S19. HR-MS (ESI) spectrum of **5**.

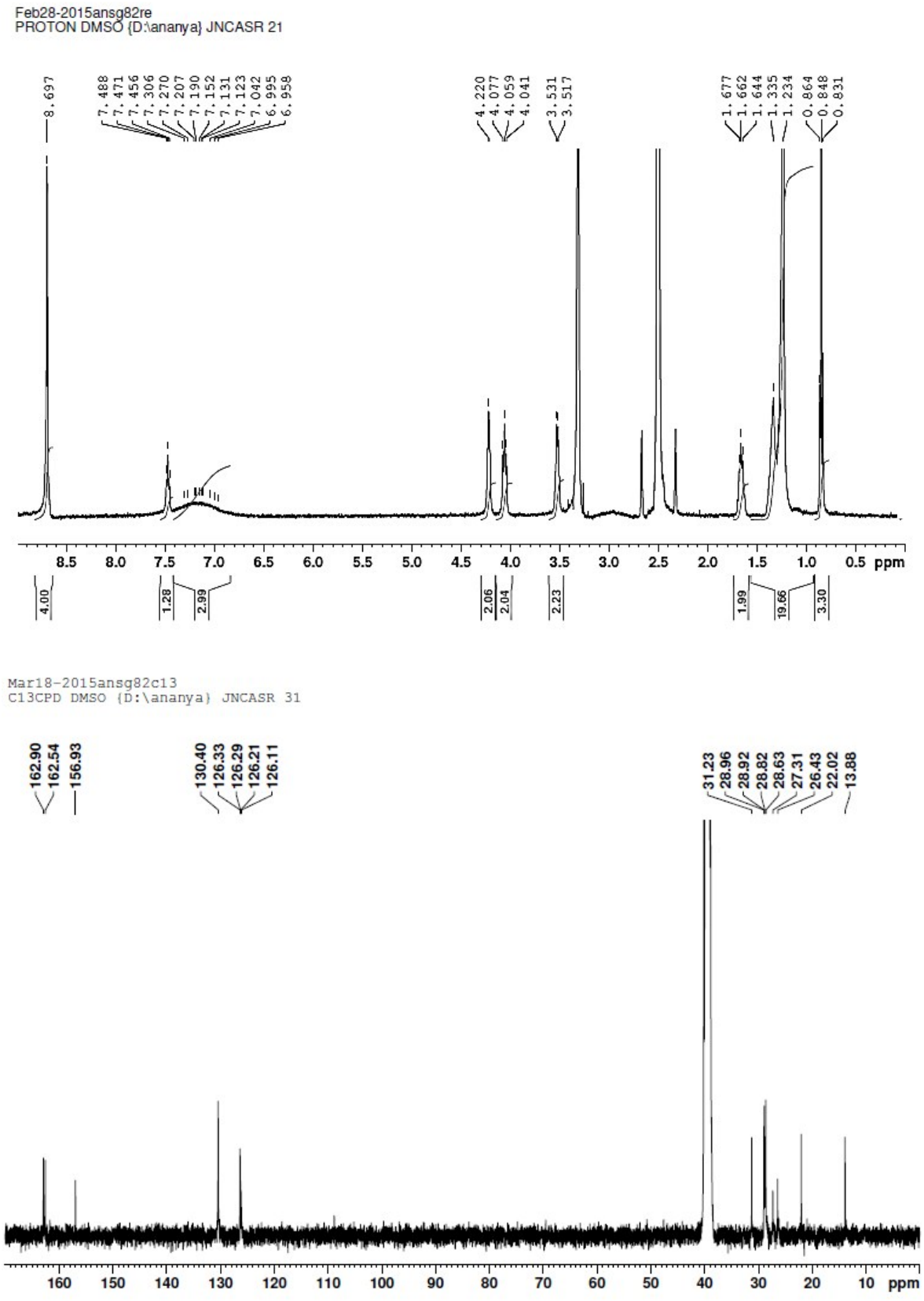

Figure S20. ^{1}H NMR and ^{13}C NMR of Boc **Amph-NDG**

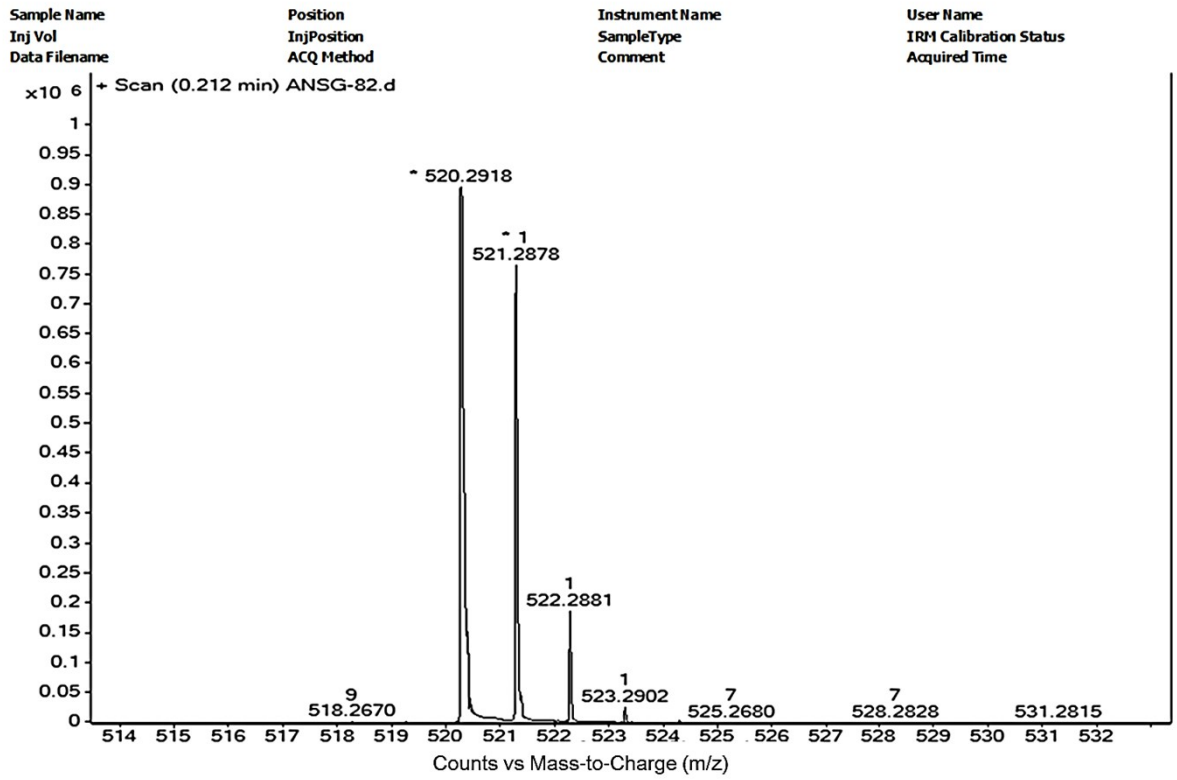

Figure S21. HR-MS (ESI) spectrum of **Amph-NDG**

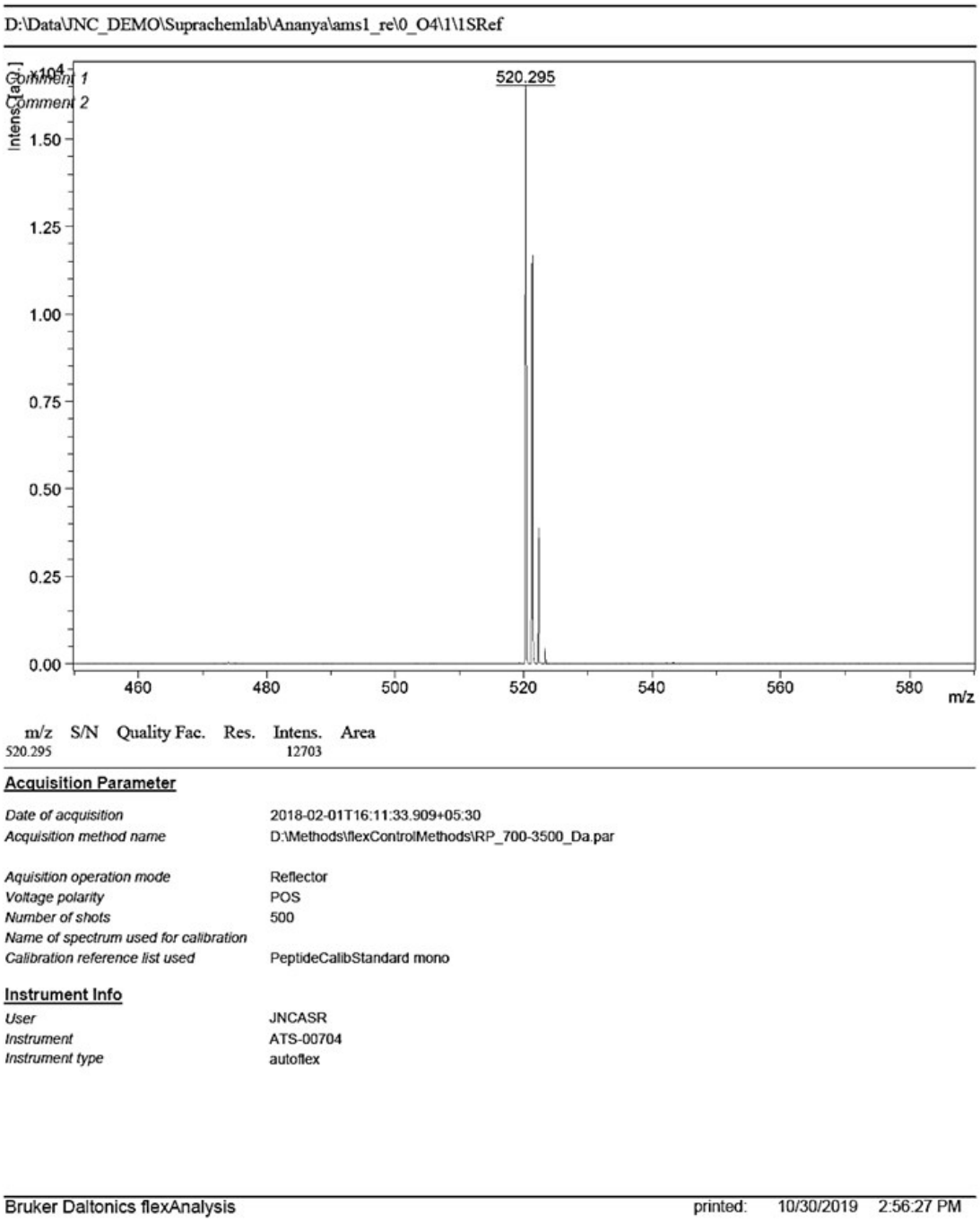

Figure S22. MALDI of **Amph-NDG**

6. References:

S . J. VandeVondele, M. Krack, F. Mohamed, M. Parrinello, T. Chassaing, J. Hutter, *Comput. Phys. Commun.,* 2005, **167**, 103-128.

S2. J. Hutter, M. Iannuzzi, F. Schiffmann, J. VandeVondele, *Wiley Interdiscip. Rev.: Comput. Mol. Sci.,* 2014, **4**, 15-25.

S3. J. P. Perdew, A. Ruzsinszky, J. Tao, V. N. Staroverov, G. E. Scuseria, G. I. Csonka, *J. Chem. Phys.,* 2005, **123**, 062201.

S4. S. Goedecker, M. Teter, J. Hutter, *Phys. Rev. B,* 1996, **54**, 1703.

S5. C. Hartwigsen, S. Goedecker, J. Hutter, *Phys. Rev. B,* 1998, **58**, 3641.

S6. S. Grimme, J. Antony, S. Ehrlich, H. Krieg, *J. Chem. Phys.,* 2010, **132**, 154104.

S7. J. Stewart, *J. Mol. Model.,* 2007, **13**, 1173-1213.

S8. A. M. Morris, M. A. Watzky, R. G. Finke, Biochim. Biophys. Acta., 2009, **1794**, 375-397.

S9. M. Frisch, G. Trucks, H. B. Schlegel, G. Scuseria, M. Robb, J. Cheeseman, G. Scalmani, V. Barone, B. Mennucci, G. Petersson, *Gaussian 09, Revision D. 01; Gaussian, Inc.: Wallingford, CT,* 2009.

S10. B. Springs, P. Haake, *Bioorg. Chem.*, 1977, **6**, 181-190; D. J. Barlow, J. M. Thornton *J. Mol. Biol.,* 1983, **168**, 867-885, R. Mogaki, P. K. Hashim, K. Okuro, T. Aida, *Chem. Soc. Rev.*, 2017, **46**, 6480-6491

S11. S. K.Shoffnera, S. Schnell, *Phys. Chem. Chem. Phys.*, 2016, **18**, 21259-21268.

S12. A. J. Markvoort, H. M. M. ten Eikelder, P. A. J. Hilbers, T. F. A. de Greef, E. W. Meijer, *Nat. Commun.*, 2011, **2**, 509; H. M. M. ten Eikelder, A. J. Markvoort, T. F. A. de Greef, P. A. J. Hilbers, *J. Phys. Chem. B*, 2012, **116**, 5291-5301.